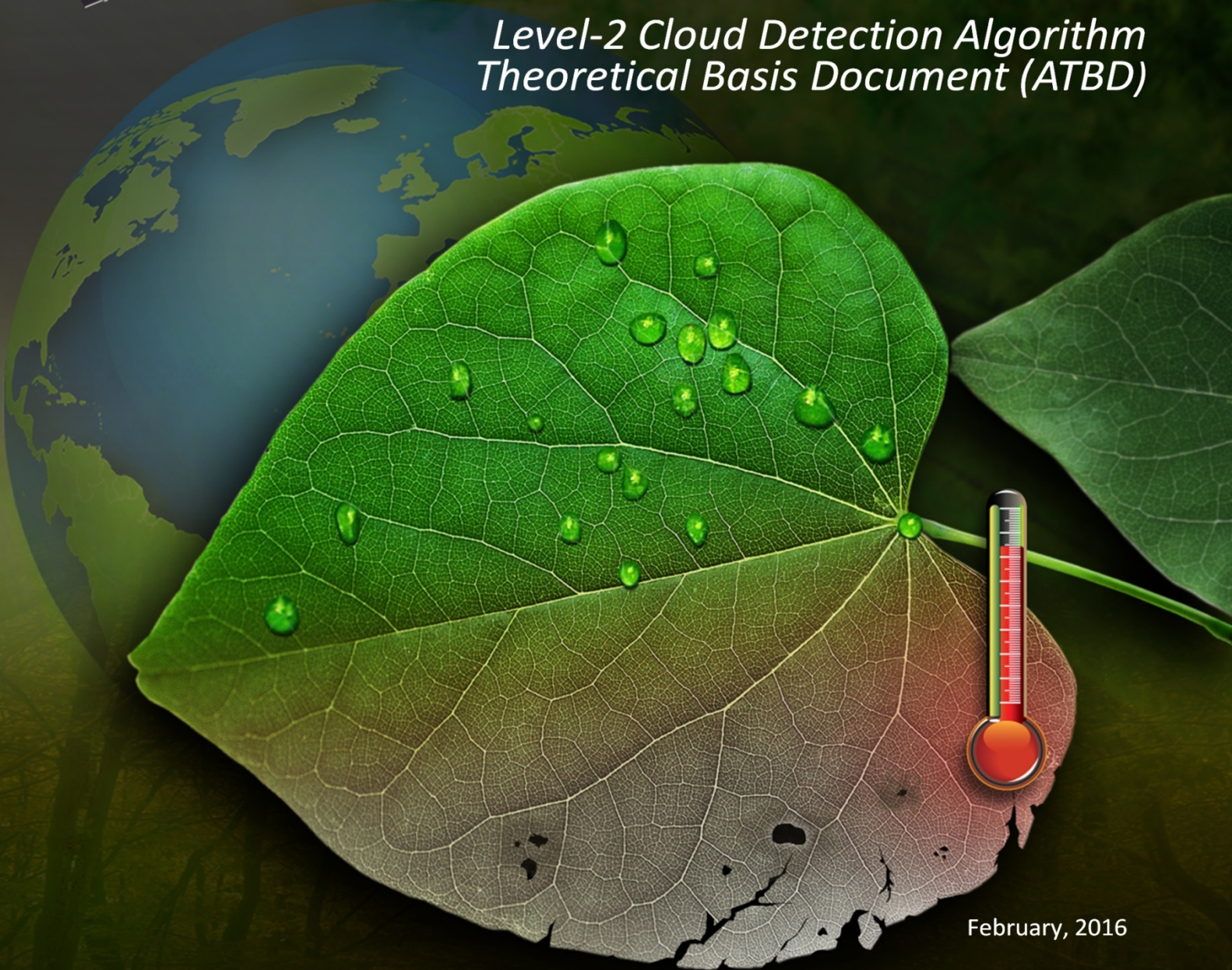




ECOSTRESS

ECOsystem Spaceborne Thermal Radiometer Experiment on Space Station

Level-2 Cloud Detection Algorithm Theoretical Basis Document (ATBD)



February, 2016

Glynn C. Hulley

Co-Investigator

Jet Propulsion Laboratory
California Institute of Technology

Simon J. Hook

Principal Investigator

Jet Propulsion Laboratory
California Institute of Technology

This research was carried out at the Jet Propulsion Laboratory, California Institute of Technology, under a contract with the National Aeronautics and Space Administration.

Reference herein to any specific commercial product, process, or service by trade name, trademark, manufacturer, or otherwise, does not constitute or imply its endorsement by the United States Government or the Jet Propulsion Laboratory, California Institute of Technology.

© 2018. California Institute of Technology. Government sponsorship acknowledged.

Change History Log

Revision	Effective Date	Prepared by	Description of Changes
Draft	02/23/2016	Glynn Hulley	ECOSTRESS L2 CLOUD ATBD first draft. Approved for public release, JPL D-94644
Version 1	02/23/2018	Glynn Hulley	Updates to cloud tests employed, output product SDS details, simulated ECOSTRESS images and cloud tests using VIIRS thermal data.
Final	06/06/2018	Glynn Hulley	Final editing

Contacts

Readers seeking additional information about this study may contact the following:

Glynn C. Hulley (Co-Investigator)

MS 183-501

Jet Propulsion Laboratory

4800 Oak Grove Dr.

Pasadena, CA 91109

Email: *glynn.hulley@jpl.nasa.gov*

Office: (818) 354-2979

Simon J. Hook (Principal Investigator)

MS 233-200

Jet Propulsion Laboratory

4800 Oak Grove Dr.

Pasadena, CA 91109

Email: *simon.j.hook@jpl.nasa.gov*

Office: (818) 354-0974

ECOSTRESS Science Team

Principal Investigator:

Simon Hook, Jet Propulsion Laboratory

Co-Investigators:

Glynn Hulley, JPL

Joshua Fisher, JPL

Rick Allen, University of Idaho

Martha Anderson, USDA

Andrew French, USDA

Eric Wood, Princeton University

Collaborators:

Christopher Hain, University of Maryland

Abstract

The ECOsystem Spaceborne Thermal Radiometer Experiment on Space Station (ECOSTRESS) mission was selected as a NASA Earth-Ventures Instrument (EV-I) Class-D mission on the International Space Station (ISS). ECOSTRESS will answer science questions related to water use and availability in several key biomes of the terrestrial biosphere using temperature information derived from the thermal infrared (TIR) measurement. The inclined, precessing ISS orbit will enable ECOSTRESS to sample the diurnal cycle in critical regions across the globe at spatiotemporal scales unexploited by current instruments in Sun-synchronous polar and high-altitude geostationary orbits. The instrument includes a TIR multispectral scanner with five spectral bands in the TIR between 8 and 12.5 μm , and leverages off the functionally-tested Prototype ECOSTRESS Thermal Infrared Radiometer (PHyTIR) space-ready hardware developed under the NASA Instrument Incubator Program. The five bands have a NE Δ T of <0.1 K at 300K and all bands have a spatial scale of 38m x 68m with a swath width of 402 km (53°). The two primary Level-2 products that will be generated by ECOSTRESS TIR data are the land surface temperature (LST) and emissivity. A critical aspect of minimizing uncertainties in these products and higher level products (L3, L4) is an accurate and reliable cloud detection and masking algorithm. This document describes the methodology behind developing the ECOSTRESS L2 Cloud Mask Algorithm (ECOCLOUD), and challenges associated with cloud detection. The ECOCLOUD algorithm derives its heritage from previously well established cloud mask algorithms such as the Landsat ACCAA, MODIS and AVHRR cloud algorithms.

Contents

Contacts	i
ECOSTRESS Science Team	ii
Abstract	iii
1 Introduction	1
2 ECOSTRESS Instrument Characteristics	4
2.1 Radiometer	5
2.2 Optics	6
3 Science Objectives	10
4 Theory and Methodology	11
4.1 Objectives.....	11
4.2 Background	11
4.3 Brightness temperature calculation	15
5 Cloud Tests	16
5.1 Test 1: Brightness Temperature Threshold.....	16
5.2 Test 2: 10.6-12 micron Brightness Temperature Difference (Thin cloud, cirrus)	17
5.3 Test 3: 8.6-10.6 micron Brightness Temperature Difference	20
5.4 Final Cloud Mask	21
6 Validation	22
6.1 Cloud mask validation strategies.....	22
6.2 Visual cloud-cover assessment (VCCA) validation procedure.....	23
7 Scientific Data Set (SDS) Variables	24
8 References	26

Figures

Figure 1: ECOSTRESS TIR instrument spectral bands from 8-12.5 micron (red) compared to ASTER (blue) and MODIS (green) with a typical atmospheric transmittance spectrum in black highlighting the atmospheric window regions.
 4

Figure 2: ECOSTRESS TIR scanning scheme 5

Figure 3: ECOSTRESS TIR conceptual layout 6

Figure 4: ECOSTRESS TIR predicted sensitivity 200–500 K..... 7

Figure 5: ECOSTRESS TIR predicted sensitivity 300–1100 K..... 7

Figure 6: ECOSTRESS number of overpasses versus overpass time at 50° latitude. 8

Figure 7: Simulated ECOSTRESS 10.6 μm band brightness temperatures (left) using VIIRS thermal data, and (right) results of the brightness temperature threshold test 1 (clouds = white pixels). 17

Figure 8: ECOSTRESS simulated brightness temperature difference between the 10.6 and 12 micron bands (left) using VIIRS thermal data, and results of the thin-cloud/cirrus test 2 (clouds = white). 18

Figure 9: Theoretical simulations of the brightness temperature difference as a function of BT11 for a cirrus cloud of varying cloud microphysical properties (image from *Ackerman et al., 2006*). 19

Figure 10: ECOSTRESS simulated brightness temperature difference between VIIRS 10.6 and 12 micron bands (left), and results of the thin-cloud/cirrus test 2 (clouds = white). 21

Figure 11: Final cloud mask image for a simulated ECOSTRESS scene using VIIRS thermal data. The final cloud mask pixels are set if any of the individual tests 1, 2, or 3 detected cloud. 22

Tables

Table 1: ECOSTRESS measurement characteristics as compared to other spaceborne TIR instruments.	3
Table 2: ECOSTRESS TIR Instrument and Measurement Characteristics	9
Table 3. Example thresholds used for BT11 threshold test in MOD35 (<i>Ackerman et al., 2006</i>).	19
Table 4. 8-bit ECOSTRESS L2 Cloud Mask Product.....	25

1 Introduction

The ECOsystem Spaceborne Thermal Radiometer Experiment on Space Station (ECOSTRESS) mission consists of a thermal infrared (TIR) multispectral scanner with one shortwave infrared (SWIR) band at 1.6 μm , and five spectral bands operating between 8 and 12.5 μm . The data in these six bands will be acquired at a spatial resolution of 38m x 68m with a swath width of 402 km (53°) from the nominal International Space Station (ISS) altitude of 400 +/- 25 km.

This document outlines the theory and methodology for generating the ECOSTRESS Level-2 Cloud Mask product. Only the five calibrated ECOSTRESS thermal bands will be used in a multispectral cloud-conservative thresholding approach. The primary purpose of the uncalibrated VSWIR band is for geolocation purposes and is not suitable for inclusion in the autonomous cloud detection algorithm since thresholds set would need to change from scene to scene. However users could still use the VSWIR data to employ their own custom cloud masks for their particular scene or use case.

Discriminating clouds is a challenging endeavor and depends on not only the type of cloud being detected, but also the type of surface over which the cloud is detected. Clouds are brighter and colder than the land surface they obscure and these properties can be exploited with the ECOSTRESS high spatial resolution TIR bands. Cloud and land surface variability, however, creates ambiguity in cloud screening. A cloud signature that works well for one scene may be ineffective for another, depending on the land surface type. Accurate cloud identification is also affected by surface features such as snow, ice, and reflective sand that have reflectance signatures similar and in some cases identical to clouds in the visible bands, especially at higher elevations. A scene dependent approach for identifying clouds has been developed for the

ECOSTRESS Cloud Mask Algorithm (ECOCLOUD) and is based primarily on cloud tests developed for the MODIS cloud algorithm (Ackerman et al. 1998).

ECOSTRESS will address critical questions on plant–water dynamics and future ecosystem changes with climate through an optimal combination of TIR measurements with high spatiotemporal and spectral resolution from the ISS. ECOSTRESS will fill a key gap in our observing capability, advance core NASA and societal objectives, and allow us to address the following science objectives: 1. Identify critical thresholds of water use and water stress in key climate sensitive biomes; 2. Detect the timing, location, and predictive factors leading to plant water uptake decline and/or cessation over the diurnal cycle; and, 3. Measure agricultural water consumptive use over the contiguous United States (CONUS) at spatiotemporal scales applicable to improve drought estimation accuracy.

These questions will be answered using the ECOSTRESS Level-3 products; Evapotranspiration (ET), Water Use Efficiency (WUE), and Evaporative Stress Index (ESI). The LST, which can be retrieved remotely from thermal infrared (TIR; 8-12.5 μm) retrievals is a necessary input to energy balance models that derive ET (Allen et al. 2007; Anderson et al. 2011; Fisher et al. 2008). Currently, there is no single satellite sensor or constellation of sensors that provide TIR data with sufficient spatial, temporal, and spectral resolution to reliably estimate ET at the global to local scale over the diurnal cycle. Measurements are either too coarse (e.g., MODIS, GOES: >1-km resolution) or infrequent (e.g., Landsat: 16-day revisit). Table 1 gives details of measurement characteristics of ECOSTRESS compared to current and future TIR missions.

Table 1: ECOSTRESS measurement characteristics as compared to other spaceborne TIR instruments.

Instrument	Platform	Resolution (m)	Revisit (days)	Daytime overpass	TIR bands (8-12.5 μm)	Launch year
ECOSTRESS	ISS	38 \times 68	3-5	Multiple	5	2018
ECOSTRESS	TBD	60	5	10:30 am	7	2024
ASTER	Terra	90	16	10:30 am	5	1999
ETM+/TIRS	Landsat 7/8	60-100	16	10:11 am	1/2	1999/2013
VIIRS	Suomi-NPP	750	Daily	1:30 am/pm	4	2011
MODIS	Terra/Aqua	1000	Daily	10:30/1:30 am/pm	3	1999/2002
GOES	Multiple	4000	Daily	Every 15 min	2	2000

The remainder of the document will discuss the ECOSTRESS instrument characteristics, provide a background on cloud detection algorithms, and show some examples of the ECOCLOUD algorithm using VIIRS simulated data.

2 ECOSTRESS Instrument Characteristics

The ECOSTRESS instrument will be implemented by placing the existing space-ready Prototype ECOSTRESS Thermal Infrared Radiometer (PHyTIR) on the ISS and using it to gather the measurements needed to address the science goals and objectives. PHyTIR was developed under the NASA Earth Science Technology Office (ESTO) Instrument Incubator Program (IIP).

The TIR instrument will acquire data from the ISS with a 38-m in-track by 68-m cross-track spatial resolution in five spectral bands, located in the TIR part of the electromagnetic spectrum between 8 and 12.5 μm shown in Figure 1. The center position and width of each band is provided in Table 2. The positions of three of the TIR bands closely match the first three thermal bands of ASTER, while two of the TIR bands match bands of ASTER and MODIS typically used for split-window type applications (ASTER bands 12–14 and MODIS bands 31, 32). It is expected that small adjustments to the band positions will be made based on ongoing engineering filter performance capabilities.

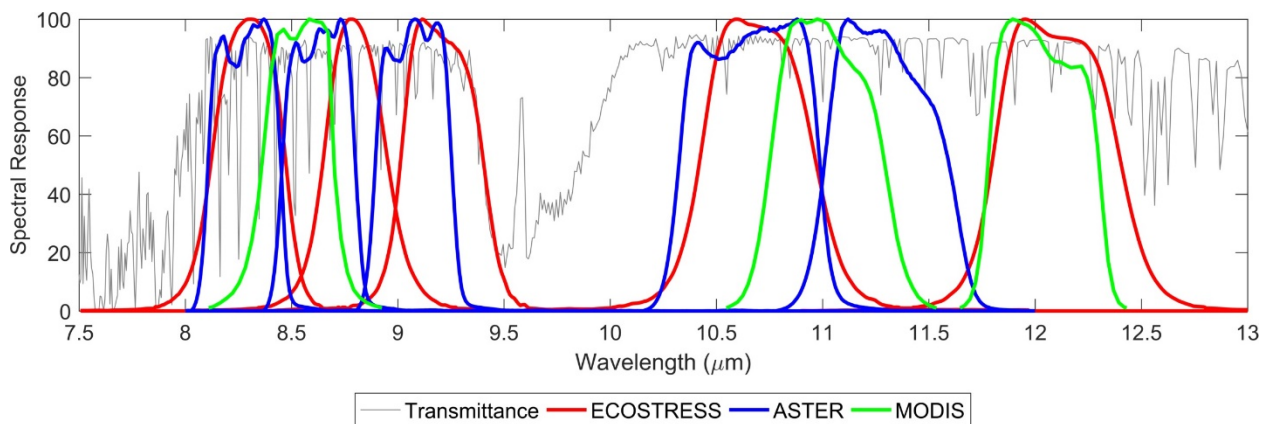


Figure 1: ECOSTRESS TIR instrument spectral bands from 8-12.5 micron (red) compared to ASTER (blue) and MODIS (green) with a typical atmospheric transmittance spectrum in black highlighting the atmospheric window regions.

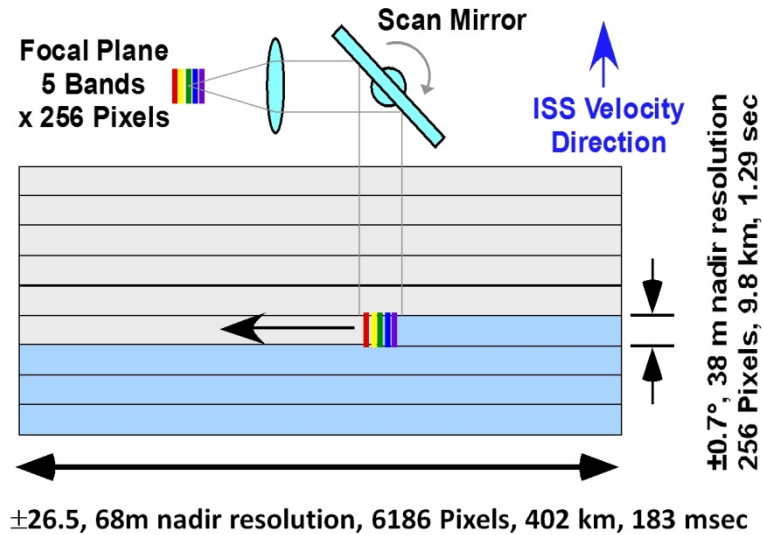


Figure 2: ECOSTRESS TIR scanning scheme

The TIR instrument will operate as a push-whisk mapper, similar to MODIS but with 256 pixels in the cross-whisk direction for each spectral channel (Figure 2), which enables a wide swath and high spatial resolution. As the ISS moves forward, the scan mirror sweeps the focal plane ground projection in the cross-track direction. Each sweep is 256-pixels wide. The different spectral bands are swept across a given point on the ground sequentially. From the 400 ± 25 -km ISS altitude, the resulting swath is 402 km wide. A wide continuous swath is produced even with an ISS yaw of up to $\pm 18.5^\circ$. A conceptual layout for the instrument is shown in Figure 3. The scan mirror rotates at a constant angular speed. It sweeps the focal plane image 53° across nadir, then to two on-board blackbody targets at 300 K and 340 K. Both blackbodies will be viewed with each cross-track sweep every 1.29 seconds to provide gain and offset calibrations.

2.1 Radiometer

The radiometer was designed and built by experienced flight hardware engineers with flight in mind. Preliminary structural analysis indicates that, with a change of the yoke material

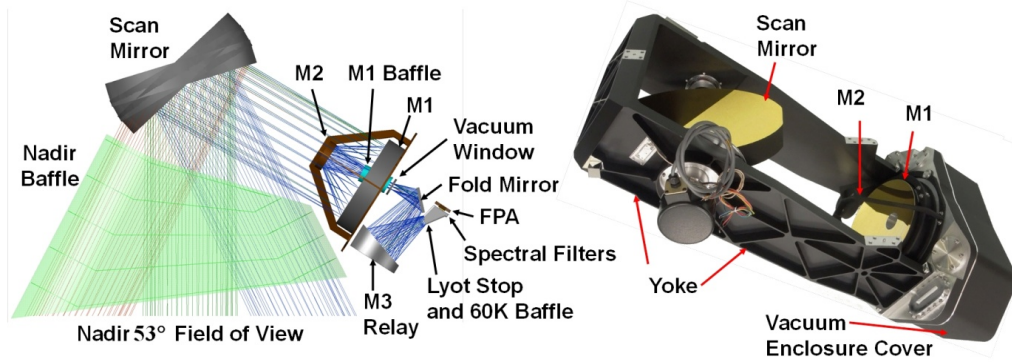


Figure 3: ECOSTRESS TIR conceptual layout

from 6061 to 7075 aluminum, the radiometer structure will have the necessary margins to withstand launch loads. Phase A-B will include a full structural analysis. The Thales LPT9310 cryocoolers will be replaced to change the welded tubing length connecting the compressors to the expanders. Also, the existing spectral filter assembly with three filters will be replaced with a new assembly containing the five filters. All replacements are straightforward, requiring only disassembly and reassembly, using standard flight procedures and documentation.

2.2 Optics

The $f/2$ optics design is all reflective, with gold-coated mirrors. The 60-K focal plane will be single-bandgap mercury cadmium telluride (HgCdTe) detector, hybridized to a CMOS readout chip, with a butcher block spectral filter assembly over the detectors. Thirty-two analog output lines, each operating at 10–12.5 MHz, will move the data to analog-to-digital converters. All the TIR channels are quantized at 14 bits. Expected sensitivities of the five channels, expressed in terms on noise-equivalent temperature difference, are shown in Figures 4 and 5. The TIR instrument will have a swath width of 402 km (53°) with a pixel spatial resolution of 38m x 68 m and it will acquire data over key climate sensitive biomes including tropical/dry transition forests and boreal forests. The large swath width of the TIR instrument combined with the

inclined, precessing ISS orbit will enable ECOSTRESS to sample at varying times throughout the day over the course of a year. Figure 6 shows an example at 50° latitude.

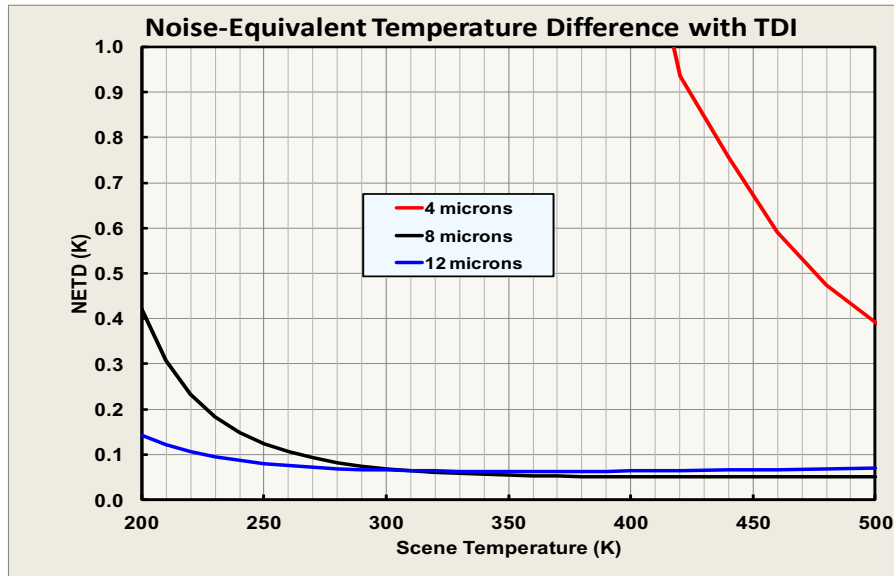


Figure 4: ECOSTRESS TIR predicted sensitivity 200–500 K.

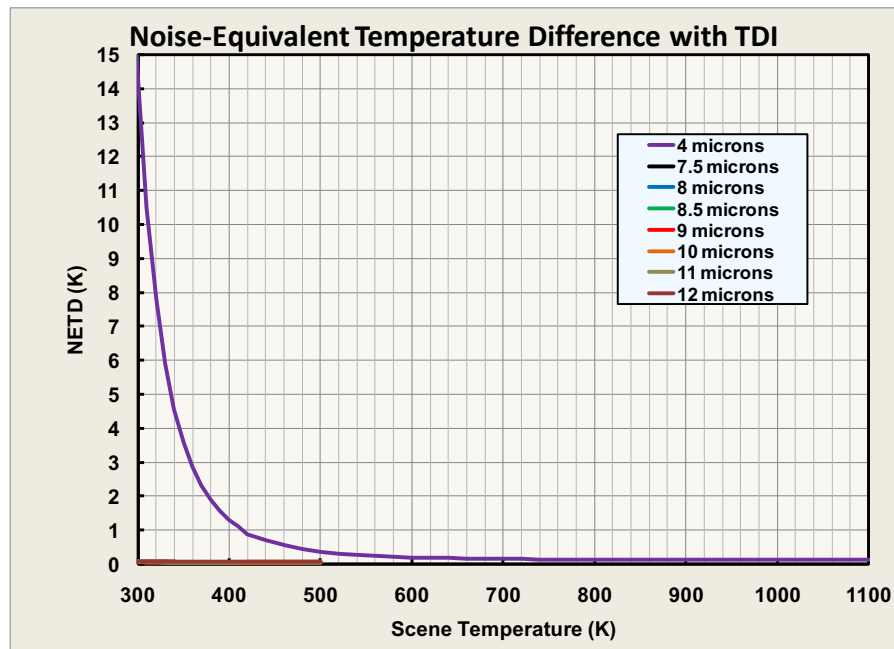


Figure 5: ECOSTRESS TIR predicted sensitivity 300–1100 K.

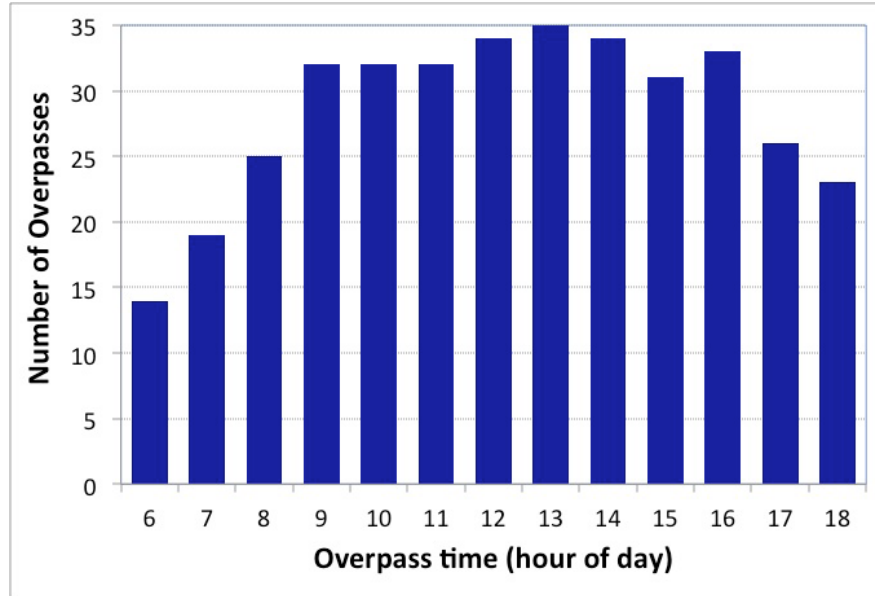


Figure 6: ECOSTRESS number of overpasses versus overpass time at 50° latitude.

Table 2: ECOSTRESS TIR Instrument and Measurement Characteristics

Spectral	
Bands (μm)	8.28, 8.63, 9.07, 11.35, 12.05
Bandwidth (μm)	0.34, 0.35, 0.36, 0.54, 0.54
Accuracy at 300 K	<0.01 μm
Radiometric	
Range	Bands 1–5 = 200 K – 500 K;
Resolution	< 0.05 K, linear quantization to 14 bits
Accuracy	< 0.5 K 3-sigma at 250 K
Precision (NE Δ T)	< 0.1 K
Linearity	>99% characterized to 0.1 %
Spatial	
IFOV	38 m in-track, 68 m cross-track
MTF	>0.65 at FNy
Scan Type	Push-Whisk
Swath Width at 400-km altitude	402 km (+/- 26.5°)
Cross Track Samples	6,186
Swath Length	9.8 km (1.29 sec)
Down Track Samples	256
Band to Band Co-Registration	0.2 pixels (12 m)
Pointing Knowledge	10 arcsec (0.5 pixels) (approximate value, currently under evaluation)
Temporal	
Orbit Crossing	Multiple
Global Land Repeat	Multiple
On Orbit Calibration	
Lunar views	1 per month {radiometric}
Blackbody views	1 per scan {radiometric}
Deep Space views	1 per scan {radiometric}
Surface Cal Experiments	2 (day/night) every 5 days {radiometric}
Spectral Surface Cal Experiments	1 per year
Data Collection	
Time Coverage	Day and Night
Land Coverage	Land surface above sea level
Water Coverage	n/a
Open Ocean	n/a
Compression	2:1 lossless

3 Science Objectives

ECOSTRESS will address critical questions on plant–water dynamics and future ecosystem changes with climate through an optimal combination of TIR measurements with high spatiotemporal resolution (38×68 m; every few days at varying times of day), and spectral resolution (5 spectral bands) from the International Space Station (ISS). The overarching goal of the ECOSTRESS is to measure water use and water stress across natural and managed ecosystems to understand vegetation change under limiting water conditions. This overarching goal will be answered by three broad questions;

- How is the terrestrial biosphere responding to changes in water availability?
- How do changes in diurnal vegetation water stress impact the global carbon cycle?
- Can agricultural vulnerability be reduced through advanced monitoring of agricultural water consumptive use and improved drought estimation?

To address these science questions, three primary objectives have been identified:

1. Identify critical thresholds of water use and water stress in key climate sensitive biomes;
2. Detect the timing, location, and predictive factors leading to plant water uptake decline and/or cessation over the diurnal cycle; and,
3. Measure agricultural water consumptive use over the contiguous United States (CONUS) at spatiotemporal scales applicable to improve drought estimation accuracy.

These science questions and objectives combine to form three core science hypotheses:

- **H1:** The WUE of a climate hotspot is significantly lower than non-hotspots of the same biome type;
- **H2:** Daily ET is overestimated when extrapolating from morning-only observations; and
- **H3:** Remotely sensed ET measured at the field scale will improve drought prediction over managed ecosystems.

4 Theory and Methodology

4.1 Objectives

The cloud mask from ECO-CLOUD will indicate whether a given view of the earth surface is unobstructed by clouds or optically thick aerosol. The cloud mask will be generated at 70-m spatial resolution. Input to ECO-CLOUD algorithm is assumed to be calibrated and geolocated L1B TIR radiance data. The cloud mask will be determined for good data only (i.e., fields of view where data in ECOSTRESS VSWIR and TIR bands have radiometric integrity). Several points need to be made regarding the approach to the ECOSTRESS cloud mask presented in this Algorithm Theoretical Basis Document (ATBD).

- (1) The cloud mask will be distributed as a separate additional L2 product, which investigators can use to screen data as appropriate for their studies.
- (2) The cloud mask ATBD assumes that calibrated, quality controlled TIR data are the input and a cloud mask is the output.
- (3) In certain heavy aerosol loading situations (e.g., dust storms, volcanic eruptions, and forest fires) particular tests may flag the aerosol-laden atmosphere as cloudy.

The final cloud mask will be output as an 8-bit mask (see Table 4), with pixel-by-pixel information on whether the cloud was determined, or not; final cloud mask, and results of three individual thermal tests, and a land/water mask. In summary, our approach to the ECOSTRESS cloud mask is, in its simplest form, to provide a binary confidence level output for each pixel.

4.2 Background

The Landsat-7 ACCA algorithm employs a rigorous approach for detecting clouds and is based on techniques used by Landsat-4 and 5 and the MODIS cloud mask. The ACCA algorithm uses eight different filters in four bands to distinguish clouds and eliminate problematic land

surfaces such as snow and highly reflective desert sands (Irish et al. 2006). The first pass through a scene uses a spectral analysis to capture cloudy pixels, while a second pass is used to develop a statistical analysis based on the Pass-1 clouds in order to identify any remaining clouds that were classed as ambiguous in the first pass. The only disadvantage of ACCA is it does not account for cloud shadows and thin cirrus.

The MODIS cloud mask (MOD35) uses 19 channels and 13 threshold-based filters to distinguish clouds (Ackerman et al. 2008; Ackerman et al. 1998). There are additionally several ancillary data inputs such as a land water map, topography, ecosystems and a snow-ice map. The algorithm is used for a wide variety of applications and provides four levels of confidence with regard to whether a pixel is clear or cloudy; confident clear (99%), probably clear (95%), uncertain clear (66%), and cloudy. The MODIS cloud mask is currently the most sophisticated in terms of the number of spectral tests used and the method of cloud classification (Ackerman et al. 2006; Frey et al. 2008). The primary drawback is the low resolution of the cloud mask (1 km), which is due to the moderate spatial resolution of the input data.

The development of the MODIS cloud mask algorithm benefited from previous work to characterize global cloud cover using satellite observations from the AVHRR (Advanced Very High Resolution Radiometer) sensor. The International Satellite Cloud Climatology Project (ISCCP) has developed cloud detection algorithms using visible/near-infrared and infrared radiances. The AVHRR Processing scheme Over cLoud Land and Ocean (APOLLO) cloud detection algorithm uses the five visible and infrared channels of the AVHRR, and the NOAA Cloud Advanced Very High Resolution Radiometer 4 (CLAVR) also uses a series of spectral visible and spatial variability tests for cloud detection.

The ISCCP cloud masking algorithm utilizes the narrowband visible (0.6 μm) and the infrared window (11 μm) channels on geostationary platform (Rossow and Duenas 2004; Rossow and Garder 1993). Observed radiances are compared with corresponding clear-sky values, and clouds are detected only when they alter the clear-sky radiances by more than the uncertainty in the clear values. Using this methodology, cloud detection thresholds are determined by the magnitude of the uncertainty in the clear radiance estimates.

The ISCCP algorithm is based on the premise that the observed visible and infrared radiances are caused by only two types of conditions, cloudy and clear, and that the ranges of radiances and their variability associated with these two conditions do not overlap (Rossow and Garder 1993). As a result, the algorithm is based upon thresholds; a pixel is classified as cloudy only if at least one radiance value is distinct from the inferred clear value by an amount larger than the uncertainty in that clear threshold value. The uncertainty can be caused both by measurement errors and by natural variability. This algorithm is constructed to be cloud-conservative, minimizing false cloud detections but missing clouds that resemble clear conditions.

The ISCCP cloud-detection algorithm consists of five steps (Rossow and Garder 1993): (1) space contrast test on a single infrared image; (2) time contrast test on three consecutive infrared images at constant diurnal phase; (3) accumulation of space/time statistics for infrared and visible images; (4) construction of clear-sky composites for infrared and visible every 5 days at each diurnal phase and location; and (5) radiance threshold for infrared and visible for each pixel.

The APOLLO scheme uses AVHRR channels 1 through 5 at full spatial resolution, nominally 1.1 km at nadir (Saunders and Kriebel 1988). The 5 spectral bandpasses are

approximately 0.58–0.68 μm , 0.72–1.10 μm , 3.55–3.93 μm , 10.3–11.3 μm , and 11.5–12.5 μm .

The technique is based on five threshold tests. A pixel is called cloudy if it is brighter or colder than a threshold, if the reflectance ratio of channels 2 to 1 is between 0.7 and 1.1, if the temperature difference between channels 4 and 5 is above a threshold, and if the spatial uniformity over ocean is greater than a threshold. These tests distinguish between cloud-free and cloudy pixels. A pixel is defined as cloud-free if the multispectral data have values below the threshold for each test. The pixel is defined as cloud-contaminated if it fails any single test, thus it is clear-sky conservative. Two of those tests are then used with different thresholds to identify cloud-filled pixels from the sub-pixel clouds.

The NOAA CLAVR algorithm (Phase I) uses all five channels of AVHRR to derive a global cloud mask (Stowe 1991). It examines multispectral information, channel differences, and spatial differences and then employs a series of sequential decision tree tests. Cloud free, mixed (sub-pixel cloud), and cloudy regions are identified for 2×2 global area coverage (GAC) pixel (4-km resolution) arrays. If all four pixels in the array fail all the cloud tests, then the array is labeled as cloud-free (0% cloudy). If all four pixels satisfy just one of the cloud tests, then the array is labeled as 100% cloudy. If 1 to 3 pixels satisfy a cloud test, then the array is labeled as mixed and assigned an arbitrary value of 50% cloudy. If all four pixels of a mixed or cloudy array satisfy a clear-restorer test (required for snow or ice, ocean specular reflection, and bright desert surfaces) then the pixel array is re-classified as “restored-clear” (0% cloudy). The set of cloud tests is subdivided into daytime ocean scenes, daytime land scenes, nighttime ocean scenes and nighttime land scenes.

Subsequent versions of CLAVR use dynamic thresholds predicted from the angular pattern observed from the clear-sky radiance statistics of the previous 9-day repeat cycle of the

NOAA satellite for a mapped one-degree equal-area grid cell. As a further modification, CLAVR will include pixel-by-pixel classification based upon different threshold tests to separate clear from cloud-contaminated pixels and to separate cloud-contaminated pixels into partial and overcast cover. Cloud contaminated pixels are classified as belonging to low stratus, thin cirrus, and deep convective cloud systems. A fourth type indicates all other clouds, including mixed level clouds.

A new cloud mask was recently developed for ASTER termed the New ASTER Cloud Mask Algorithm (NACMA) (Hulley and Hook 2008). The algorithm was developed by selecting key tests from the Landsat-7, MODIS, and AVHRR algorithms highlighted above. Using this approach a hybrid cloud detection algorithm that capitalized on the previous approaches was developed. For identifying clear-pixels for surface parameter datasets, the cloud mask was designed to be clear-sky conservative (i.e., overestimate rather than underestimate the amount of cloud), and filter threshold values were adjusted to account for this. Additionally, a cloud-filling technique was used to fill in gaps between clouds and shadows. For the ECOCLOUD algorithm, we plan on using three thermal infrared spectral tests based on heritage from MODIS and AVHRR and described in the following sections.

4.3 Brightness temperature calculation

Theoretically, brightness temperatures for each ECOSTRESS band can be calculated on a pixel-by-pixel basis by inverting the Planck equation:

$$T_b(\lambda) = \frac{c2}{\lambda \cdot \ln\left(\frac{c1}{\lambda^5 \cdot \pi \cdot L_\lambda} + 1\right)} \quad (1)$$

where:

λ is wavelength in μm ,

$$c1 = 0.0143877$$

$$c2 = 3.741775e-22$$

L_2 is the at-sensor spectral radiance in $W/(m^2 \cdot sr \cdot \mu m)$

However, this formulation will increasingly become inaccurate for a sensor's spectral response that deviates from delta function behavior. Instead, we use a look up table (LUT) approach in which the Planck function is used to compute expected radiances for each respective ECOSTRESS band's spectral response functions over a range of temperatures in 0.01 K intervals that encompass the full range of expected Earth-like temperatures (typically 150 to 380 K). This results in a table of values of radiances versus temperatures for each given sensor. The table can then simply be 'inverted' by interpolating to get the desired temperature. The table can be modified to any desired precision by decreasing the step size interval (e.g. from 0.01 to 0.001 K).

5 Cloud Tests

ECOCLOUD will use all available thermal tests currently used by the MODIS and VIIRS cloud mask algorithms. These include a threshold based on 11 micron brightness temperature, and two thermal difference tests based on differences between the 10.6 and 12 micron bands, and the 8.6 and 10.6 micron bands.

5.1 Test 1: Brightness Temperature Threshold

This filter examines the thermal band 11 μm brightness temperature (BT11), to flag potential cloud pixels. A realistic cloud brightness temperature maximum over land is usually 300 K, but this may change depending on the surface type. To account for temperature changes with elevation, the ASTER Digital Elevation Model (DEM) is used along with a standard lapse rate (6 K/km) to calculate an estimate of the threshold, i.e., if the brightness temperature is

greater than $300 \text{ K} - 6 * \text{DEM (km)}$, then it is excluded and labeled as non-cloud in the mask.

Figure 7 shows an example of simulated ECOSTRESS $10.6 \mu\text{m}$ band brightness temperatures using VIIRS thermal data from the M15 band for a scene over southern california, and (right) results of the brightness temperature threshold test 1 (clouds = white pixels).

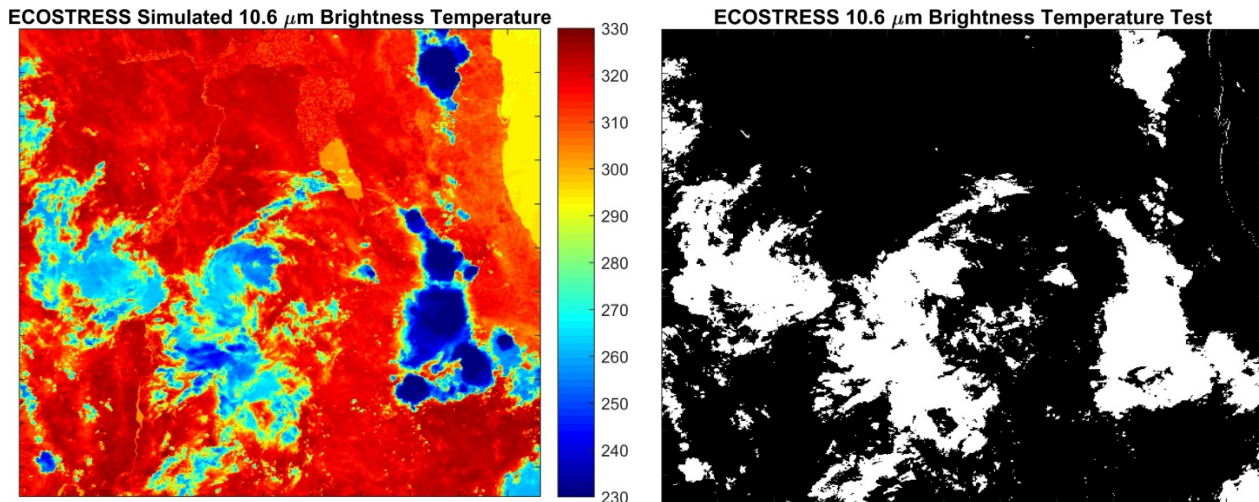


Figure 7. Simulated ECOSTRESS $10.6 \mu\text{m}$ band brightness temperatures (left) using VIIRS thermal data, and (right) results of the brightness temperature threshold test 1 (clouds = white pixels).

5.2 Test 2: 10.6-12 micron Brightness Temperature Difference (Thin cloud, cirrus)

The thin-cloud/cirrus test utilizes a brightness temperature difference test between two longwave thermal bands (e.g., 11 and $12 \mu\text{m}$) and works well for thin cirrus, the edges of thicker cloud, low reflectance clouds and a variety of other types of cloud. Differences between BT11 and BT12 are widely used for cloud screening with AVHRR and GOES measurements, and this technique is often referred to as the split window technique. *Saunders and Kriebel (1988)* used BT11–BT12 differences to detect cirrus clouds—brightness temperature differences are larger over thin clouds than over clear or overcast conditions and arise due to the different emissivities of the cloud at the two wavelengths as a result of the non-linear nature of the Planck function. In

the MODIS cloud mask, thresholds were set as a function of satellite zenith angle and the BT11 brightness temperature.

In the ASTER cloud mask algorithm (Hulley and Hook 2008), the thresholds are computed by looking at BT11–BT12 differences for a variety of clear-sky scenes over varying terrain features including desert, mountainous terrain, and vegetation. For clear sky conditions, the differences should be less than 1 K, but could be as large as 6 K for cloudy conditions. The maximum differences are then noted and used to set appropriate thresholds. For a pixel with

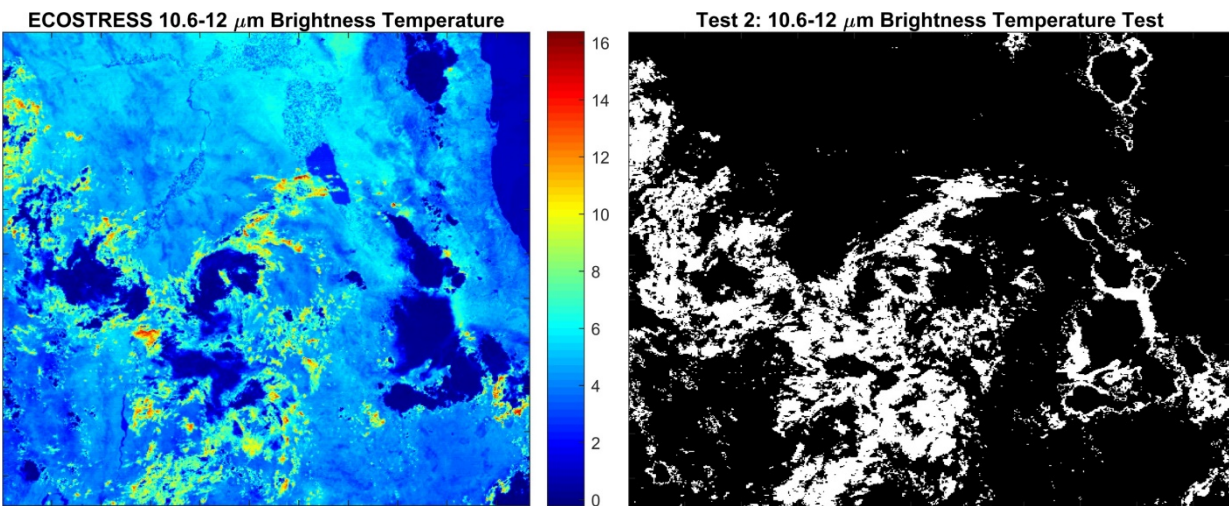


Figure 8. ECOSTRESS simulated brightness temperature difference between the 10.6 and 12 micron bands (left) using VIIRS thermal data, and results of the thin-cloud/cirrus test 2 (clouds = white).

given BT11, BT differences greater than the threshold values are classified as cloud. A similar procedure will be used for ECOSTRESS and an example of this test using VIIRS thermal data is demonstrated in Figure 8, which shows ECOSTRESS simulated brightness temperature difference between the 10.6 and 12 micron bands, and results of the thin-cloud/cirrus test 2 (clouds = white pixels).

Figure 9 shows an example of a theoretical simulation of the brightness temperature difference between 11 and 12 μm versus the brightness temperature at 11 μm , assuming a standard tropical atmosphere (Ackerman et al. 2006). The difference is a function of cloud optical thickness, the cloud temperature, and the cloud particle size distribution. The difficulty in using these tests for cloud detection is often defining the clear-sky value on this type of diagram. Table 3 shows example thresholds based on figure 6 for the MODIS cloud mask algorithm (Ackerman et al. 2006). ECOSTRESS thresholds will be estimated using a variety of different simulations over different land surfaces and similar results from Figure 12.

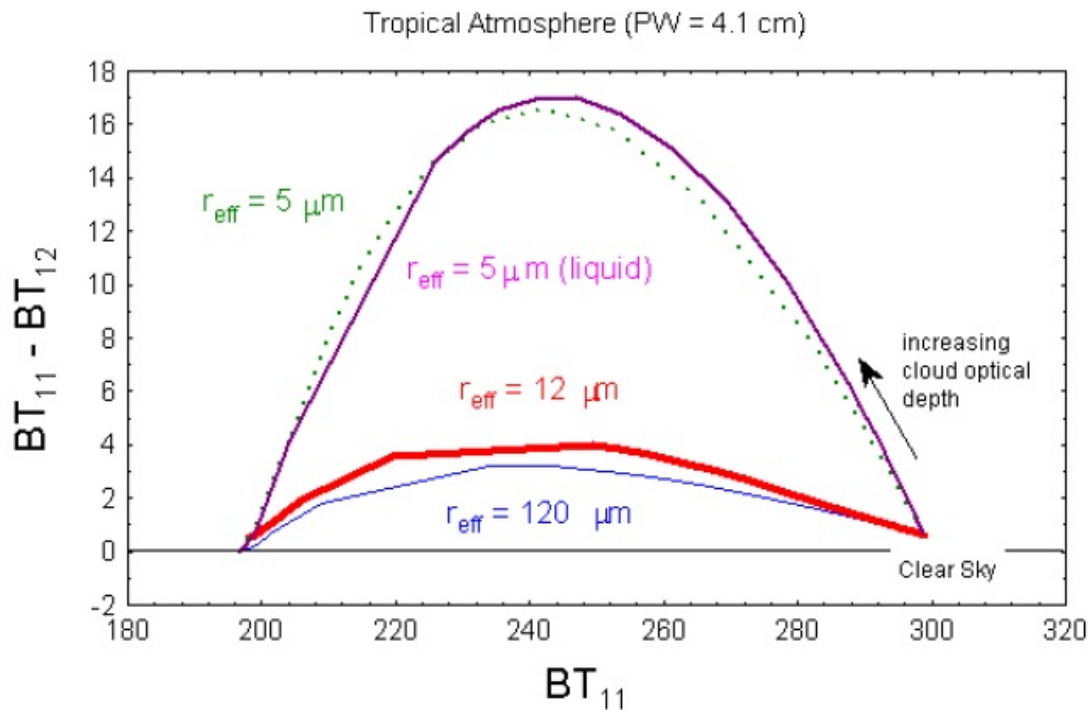


Figure 9. Theoretical simulations of the brightness temperature difference as a function of BT11 for a cirrus cloud of varying cloud microphysical properties (image from Ackerman et al., 2006).

Table 3. Example thresholds used for BT11 threshold test in MOD35 (Ackerman et al., 2006).

Scene Type	Threshold	High confidence clear	Low confidence clear
Day ocean	270 K	273 K	267 K

Night ocean	270 K	273 K	267 K
Day land	297.5 K	302.5 K	NA
Night land	292.5 K	297.5 K	NA
Night desert	292.5K	297.5 K	NA
Day Desert	292.5K	302.5 K	NA

5.3 Test 3: 8.6-10.6 micron Brightness Temperature Difference

The basis for the 8.6-10.6 micron brightness temperature difference test is the same as that of the 10.6-12 micron split window test, and lies in the differential water vapor absorption that exists between different window channels (8.6 and 10.6 μm and 10.6 and 12 μm) where absorption is relatively weak. The strongest absorbing molecule in these regions is a result of atmospheric water vapor content, with a minimum occurring around 11 μm . Figure 10 shows an example of ECOSTRESS simulated brightness temperature difference between the 8.6 and 10.6 micron bands, and results of test 3 (clouds = white pixels). Note how brightness temperatures have large negative values over land, but have positive values over cloud. We have found that a threshold setting of -1 is optimal for detecting most cloud using this test.

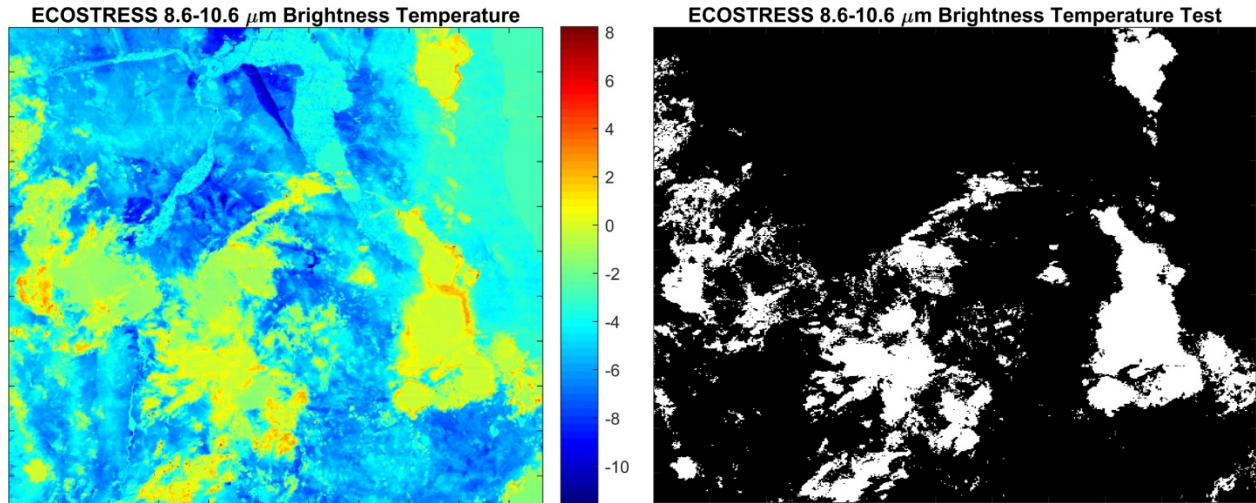


Figure 10. ECOSTRESS simulated brightness temperature difference between VIIRS 10.6 and 12 micron bands (left), and results of the thin-cloud/cirrus test 2 (clouds = white).

5.4 Final Cloud Mask

The final cloud mask is simply an ‘or’ of the three thermal tests. This maximizes the cloud detection and takes advantage of the unique capabilities for each test, for example the brightness temperature threshold test may miss areas of thin cloud and/or cirrus during colder temperatures, or over snow covered regions. However, results of each individual test are also output in the final 8-bit cloud mask product (see Table 4), to give users the freedom of using the cloud test results as needed, or for particular conditions. For example, over colder environments test 1 may overestimate the amount of cloud detected, in which cases users should rely more on tests 2 and 3.

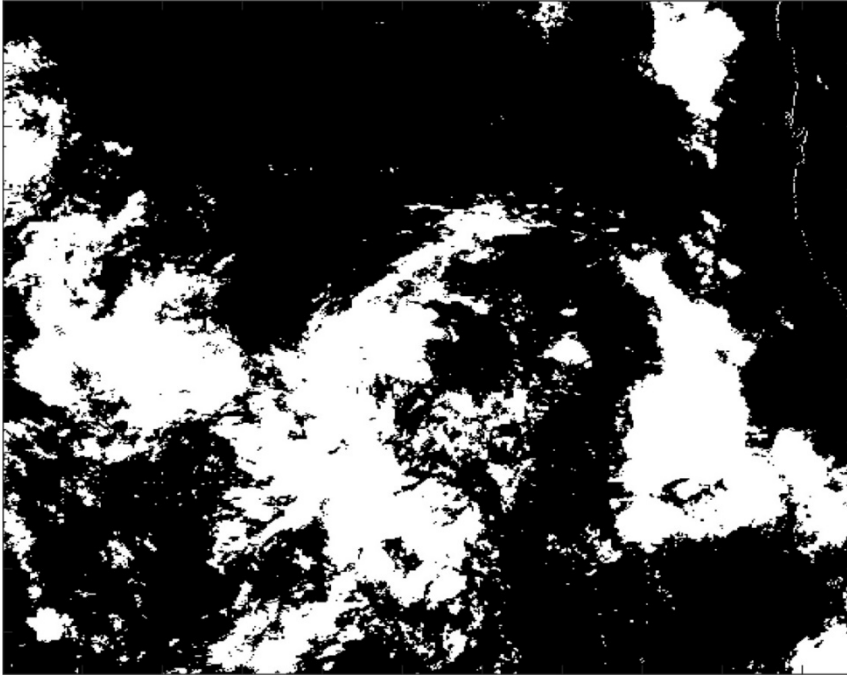
ECOSTRESS Final Cloud Mask

Figure 11. Final cloud mask image for a simulated ECOSTRESS scene using VIIRS thermal data. The final cloud mask pixels are set if any of the individual tests 1, 2, or 3 detected cloud.

6 Validation

For validation of the ECOSTRESS cloud mask, once enough data is acquired, several difficult-case-scenario scenes will be chosen over different land cover types and for a variety of cloud types. A visual cloud cover assessment (VCCA) will be the primary tool for evaluating the quality of the cloud mask, supplemented by a statistical approach for assessing the total cloud cover on each scene.

6.1 Cloud mask validation strategies

Following the first few years of Landsat 7 operations, the Landsat Project Science Office (LPSO) staff undertook a validation of all elements of the Long-Term Acquisition Plan (LTAP) including the ACCA algorithm (Markham and Barker 1986). The approach chosen to validate Landsat ACCA performance, and which we will use for ECOSTRESS, is a supervised

classification of a stratified sample of global scenes using three-band (R,G,B) browse imagery for comparison to corresponding ECOCLLOUD mask outputs. For Landsat, B5, B4, and B3 were used to define the red (R), green (G), and blue (B) elements respectively for the browse images. A linear contrast stretch was applied to each browse image to ensure adequate contrast in the RGB product. A reduced-resolution browse-scene approach to assessing cloud cover (CC) is feasible because both ACCA and ECOCLLOUD will output a single cloud scene percentage for the entire scene. Furthermore, the ACCA definition of clouds as nearly opaque and the ability to visually compare the supervised classification of browse imagery to adjacent scenes and other dates allowed an iterative and precise analysis approach. This VCCA will be used as a measure of the true CC in the scene.

6.2 Visual cloud-cover assessment (VCCA) validation procedure

Supervised classification will be performed using a procedure described in (Irish et al. 2006). Calculations will be performed using Adobe® Photoshop® image processing software. The *magic wand* and *freehand lasso* tools of Photoshop® will be used to isolate clouds in the respective RGB browse images. The wand employs a seed-fill threshold algorithm to compute regions of brightness similarity based on a mouse click of a single pixel. The algorithm compares the selected pixel's brightness values to all other pixels and retains those within a selectable tolerance threshold. For example, clicking on an RGB-browse-image pixel with values R:200, G:220, and B:240 and a tolerance set to 5, results in selection of pixels in the ranges: $195 < R < 205$, $215 < G < 225$, and $235 < B < 245$. Additional cloud pixels will be added by using the wand repeatedly until the cumulative selection of visible clouds had essentially zero possibility of VCCA omission errors. Snowfields and other unwanted bright features will be manually subtracted using the lasso tool to reduce VCCA commission errors. After the VCCA scores are

established, the resulting cloud pixels will be filled with zeros and all others a value of one. The result will be a binary cloud mask that allowed a CC percentage computation serving as the cloud “truth” for validating the accuracy of the official ECO-CLOUD cloud mask.

7 Scientific Data Set (SDS) Variables

The ECOSTRESS L2 Cloud Mask product will be archived in Hierarchical Data Format 5 - Earth Observing System (HDF5-EOS) format files. HDF is the standard archive format for NASA EOS Data Information System (EOSDIS) products. The L2 Cloud files will contain global attributes described in the metadata, and scientific data sets (SDSs) with local attributes. Unique in HDF-EOS data files is the use of HDF features to create point, swath, and grid structures to support geolocation of data. These structures (Vgroups and Vdata) provide geolocation relationships between data in an SDS and geographic coordinates (latitude and longitude or map projections) to support mapping the data. Attributes (metadata), global and local, provide various information about the data. Users unfamiliar with HDF and HDF-EOS formats may wish to consult Web sites listed in the Related Web Sites section for more information.

The Cloud Mask SDS contains the 8 bit cloud mask product. A bit-by-bit description of the ECOSTRESS Cloud Mask SDS is provided in Table 4. Any additional metadata necessary for describing the product including quality, test implementation information as well as a record of what ancillary data sets were used in the generation of the product for each individual field-of-view will be included in the product specific metadata.

Table 4. 8-bit ECOSTRESS L2 Cloud Mask Product.

Bit Field	Long Name	Result
0	Cloud Mask Flag	0 = not determined 1 = determined
1	Cloud, either one of bits 2, 3, or 4 set.	0 = no 1 = yes
2	Thermal Brightness Test	0 = no 1 = yes
3	Band 4-5 Thermal Difference test	0 = no 1 = yes
4	Band 2-5 Thermal Difference test	0 = no 1 = yes
5	land/water mask	0 = land 1 = water

8 References

- Ackerman, S., Strabala, K.I., Menzel, P., Frey, R., Moeller, C.C., Gumley, L.E., Baum, B., Seemann, S.W., & Zhang, H. (2006). Discriminating clear-sky from cloud with MODIS algorithm theoretical basis document (MOD35), *Cooperative Institute for Meteorological Satellite Studies, University of Wisconsin-Madison, NOAA/NESDIS, version 5.0, October 2006*
- Ackerman, S.A., Holz, R.E., Frey, R., Eloranta, E.W., Maddux, B.C., & McGill, M. (2008). Cloud detection with MODIS. Part II: Validation. *Journal of Atmospheric and Oceanic Technology*, 25, 1073-1086
- Ackerman, S.A., Strabala, K.I., Menzel, W.P., Frey, R.A., Moeller, C.C., & Gumley, L.E. (1998). Discriminating clear sky from clouds with MODIS. *Journal of Geophysical Research-Atmospheres*, 103, 32141-32157
- Allen, R.G., Tasumi, M., & Trezza, R. (2007). Satellite-based energy balance for mapping evapotranspiration with internalized calibration (METRIC) - Model. *Journal of Irrigation and Drainage Engineering-Asce*, 133, 380-394
- Anderson, M.C., Kustas, W.P., Norman, J.M., Hain, C.R., Mecikalski, J.R., Schultz, L., Gonzalez-Dugo, M.P., Cammalleri, C., d'Urso, G., Pimstein, A., & Gao, F. (2011). Mapping daily evapotranspiration at field to continental scales using geostationary and polar orbiting satellite imagery. *Hydrology and Earth System Sciences*, 15, 223-239
- Fisher, J.B., Tu, K.P., & Baldocchi, D.D. (2008). Global estimates of the land-atmosphere water flux based on monthly AVHRR and ISLSCP-II data, validated at 16 FLUXNET sites. *Remote Sensing of Environment*, 112, 901-919
- Frey, R.A., Ackerman, S.A., Liu, Y.H., Strabala, K.I., Zhang, H., Key, J.R., & Wang, X.G. (2008). Cloud detection with MODIS. Part I: Improvements in the MODIS cloud mask for collection 5. *Journal of Atmospheric and Oceanic Technology*, 25, 1057-1072
- Hulley, G.C., & Hook, S.J. (2008). A new methodology for cloud detection and classification with ASTER data. *Geophysical Research Letters*, 35, L16812, doi: 16810.11029/12008gl034644
- Irish, R.R., Barker, J.L., Goward, S.N., & Arvidson, T. (2006). Characterization of the Landsat-7 ETM+ automated cloud-cover assessment (ACCA) algorithm. *Photogrammetric Engineering and Remote Sensing*, 72, 1179-1188
- Markham, B.L., & Barker, J.L. (1986). Landsat MSS & TM Post-Calibration Dynamic Ranges, Exoatmospheric Reflectances & At-Satellite Temperatures. In, *EOSAT Landsat Technical Notes, No. 1*.
- Rossow, W.B., & Duenas, E.N. (2004). The International Satellite Cloud Climatology Project (ISCCP) Web site - An online resource for research. *Bulletin of the American Meteorological Society*, 85, 167-172
- Rossow, W.B., & Garder, L.C. (1993). Cloud Detection Using Satellite Measurements of Infrared and Visible Radiances for Isccp. *Journal of Climate*, 6, 2341-2369
- Saunders, R.W., & Kriebel, K.T. (1988). An Improved Method for Detecting Clear Sky and Cloudy Radiances from Avhrr Data. *International Journal of Remote Sensing*, 9, 123-150
- Stowe, L.L. (1991). Cloud and Aerosol Products at Noaa Nesdis. *Global and Planetary Change*, 90, 25-32